Report

Cell Reports

Mechano-Dependent Phosphorylation of the PDZ-Binding Motif of CD97/ADGRE5 Modulates Cellular Detachment

Graphical Abstract

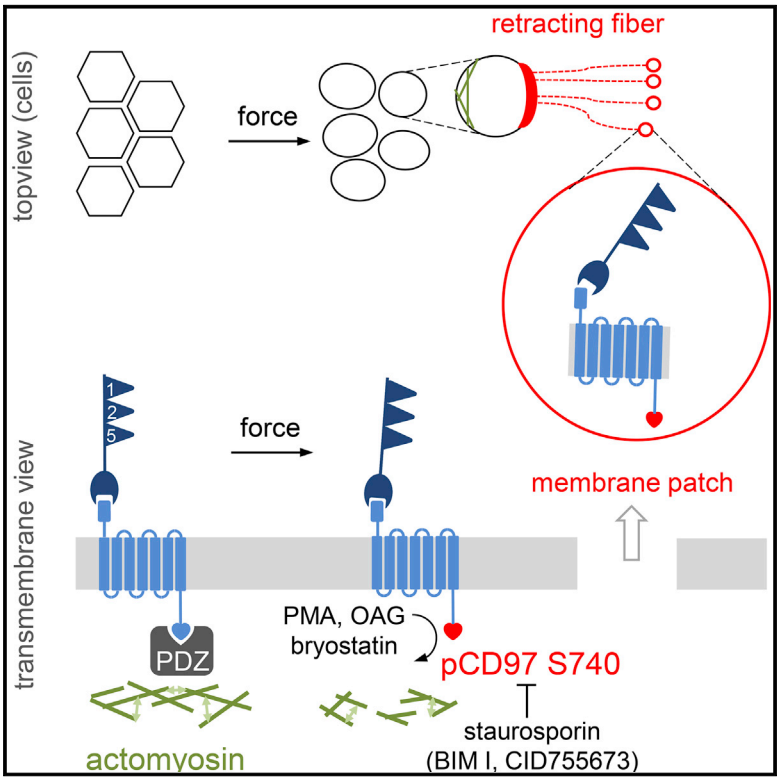

Highlights

- Phosphorylation of S740 in the PDZ-binding motif (PBM) of CD97 alters its binding
- Mechanical force-induced phospho-CD97 at S740 facilitates (intra)cellular detachment
- Protein kinases C and D can phosphorylate CD97 at S740
- PBM- and GNA12/13-mediated signaling of CD97 are partly independent

Authors

Doris Hilbig, Doreen Sittig, Franz Hoffmann, ..., Josef A. Käs, Lawrence Banks, Gabriela Aust

Correspondence

gabriela.aust@medizin.uni-leipzig.de

In Brief

Adhesion GPCRs are potential mechanoreceptors. Hilbig et al. demonstrate that CD97/ADGRE5 shapes the cellular mechanoresponse by modulating signaling at its intracellular tail. Mechanical stimuli rapidly induce phosphorylation in the CD97 C-terminal PDZ-binding motif, which alters the intracellular coupling of the receptor, thereby affecting cellular viscoelastic properties and detachment.

Hilbig et al., 2018, Cell Reports *24*, 1986–1995
August 21, 2018
https://doi.org/10.1016/j.celrep.2018.07.071

CellPress

OPEN ACCESS
CellPress

Cell Reports
Report

Mechano-Dependent Phosphorylation of the PDZ-Binding Motif of CD97/ADGRE5 Modulates Cellular Detachment

Doris Hilbig,[1] Doreen Sittig,[1] Franz Hoffmann,[1] Sven Rothemund,[2] Enrico Warmt,[3] Marianne Quaas,[1] Julia Stürmer,[1] Liane Seiler,[4] Ines Liebscher,[4] Ngoc Anh Hoang,[1] Josef A. Käs,[3] Lawrence Banks,[5] and Gabriela Aust[1,6,*]

[1]Department of Surgery, Research Laboratories, Leipzig University, Leipzig, Germany
[2]Core Unit Peptide-Technologies, Leipzig University, Leipzig, Germany
[3]Peter Debye Institute for Soft Matter Physics, Leipzig University, Leipzig, Germany
[4]Rudolf Schönheimer Institute of Biochemistry, Leipzig University, Leipzig, Germany
[5]International Centre for Genetic Engineering and Biotechnology, Trieste, Italy
[6]Lead Contact
*Correspondence: gabriela.aust@medizin.uni-leipzig.de
https://doi.org/10.1016/j.celrep.2018.07.071

SUMMARY

Cells respond to mechanical stimuli with altered signaling networks. Here, we show that mechanical forces rapidly induce phosphorylation of CD97/ADGRE5 (pCD97) at its intracellular C-terminal PDZ-binding motif (PBM). Biochemically, this phosphorylation disrupts CD97 binding to PDZ domains of the scaffold protein DLG1. In shear-stressed cells, pCD97 appears not only in junctions, retracting fibers, and the attachment area but also in lost membrane patches, demonstrating (intra)cellular detachment at the CD97 PBM. This motif is critical for the CD97-dependent mechanoresponse. Cells expressing CD97 without the PBM are more deformable, and under shear stress, these cells lose cell contacts faster and show changes in the actin cytoskeleton when compared with cells expressing full-length CD97. Our data indicate CD97 linkage to the cytoskeleton. Consistently, CD97 knockout phenocopies CD97 without the PBM, and membranous CD97 is organized in an F-actin-dependent manner. In summary, CD97 shapes the cellular mechanoresponse through signaling modulation via its PBM.

INTRODUCTION

Mechanoreceptors sense and transduce mechanical stimuli into altered biochemical processes such as protein unbinding or protein conformational changes, which in turn shape the cellular response (Hoffman et al., 2011). Several adhesion G protein-coupled receptors (aGPCRs) have been identified as potential metabotropic mechanoreceptors (Scholz et al., 2015; Petersen et al., 2015; Wilde et al., 2016; Boyden et al., 2016). Missense mutations in EMR2/ADGRE2 cause vibratory urticaria, a skin disease in which cutaneous vibration leads to hives (Boyden et al., 2016). The closely related homolog of EMR2, CD97/ADGRE5, is present in many cells that are subjected to mechanical forces, such as normal and malignant intestinal and lung epithelial and muscle cells, as well as leukocytes.

CD97 combines the typical structural features of aGPCRs (Figure 1A). The large extracellular domain (ECD), consisting of tandemly arranged adhesive epidermal growth factor (EGF)-like folds plus the juxtamembrane GPCR autoproteolysis-inducing (GAIN) domain, is connected to the seven-span transmembrane helices followed by the intracellular domain (ICD), which terminates in a PSD-95/discs-large/ZO-1 (PDZ)-binding motif (PBM) with the sequence ASESGI. PBMs, present in one-third of human aGPCRs (Langenhan et al., 2013), bind to the PDZ domains of scaffold proteins, thereby positioning transmembrane receptors correctly within protein networks at cellular junctions and connecting them to intracellular signaling networks. The GAIN domain contains an autocatalytic GPCR proteolysis site (GPS), which cleaves CD97 into the N-terminal fragment (NTF) and C-terminal fragment (CTF).

The observation that deletion of the NTF increases basal activity of several aGPCRs (Okajima et al., 2010; Paavola et al., 2011; Ward et al., 2011) has led to efforts to understand their activation. Not shown for CD97, but present in many aGPCRs, the very N-terminal part of the CTF carries the tethered agonist, the so-called *Stachel*, which is suggested to be a mechanosensitive structure of aGPCRs (Liebscher et al., 2014; Petersen et al., 2015; Stoveken et al., 2015; Wilde et al., 2016). Mechanoactivation of the *Drosophila* aGPCR dCirl depends on the intact *Stachel* sequence, whereas cleavage is dispensable (Scholz et al., 2017). However, signaling of aGPCRs is multifaceted and does not necessarily depend on a *Stachel* sequence (Kishore et al., 2016; Salzman et al., 2016, 2017).

Here, we examined CD97 signaling in the context of mechanotransduction. Mechanical stimuli rapidly induced phosphorylation of Ser740 (S740) in the intracellular CD97 PBM, which disrupted its binding to PDZ domains of the scaffold protein DLG1 at the biochemical level. We defined the PBM as a critical structure for the CD97-dependent cellular mechanoresponse.

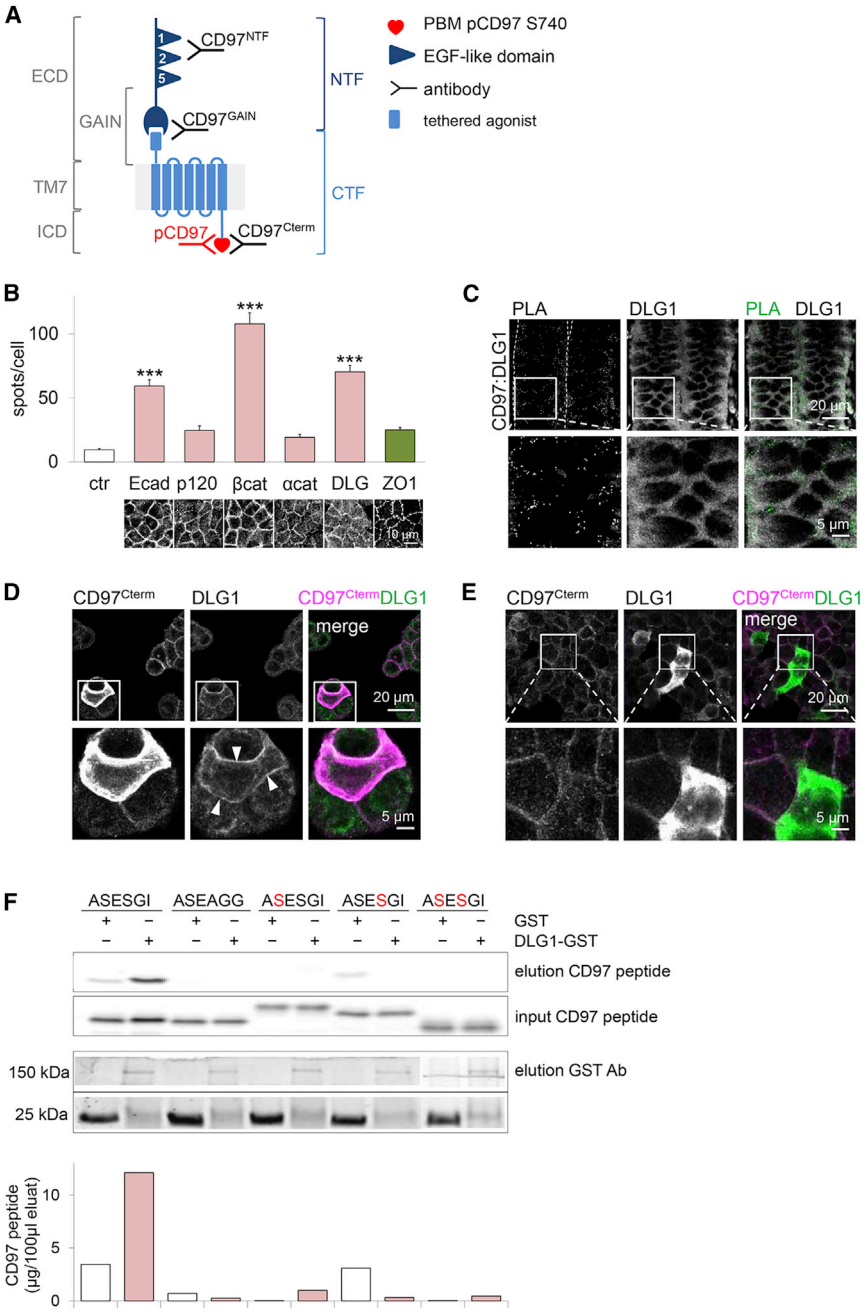

Figure 1. CD97 Binds through Its PBM to DLG1

(A) Schema of the shortest CD97 isoform with three EGF-like folds (EGF125) and binding sites of the CD97-specific Abs used in the study. For explanations, see the main text.

(B) CD97 co-localized with junctional proteins in monolayers of colorectal DLD1 cells. Upper: the number of proximity ligation assay (PLA) interaction spots per cell was counted. n = 50 cells, mean ± SEM; ***p < 0.001 compared with ZO1, a tight junction protein. Lower: images of the cells stained with Abs directed to the proteins examined. Ecad, E-cadherin; p120, p120 catenin; βcat, β-catenin; αcat, α-catenin.

(C) In normal human colon, interaction of CD97 and DLG1, seen as interaction spots in the assay, was restricted to the lateral cellular junction of enterocytes; the sections were stained after the PLA with a fluorophore-labeled secondary Ab to visualize DLG1.

(D and E) CD97-enriched DLG1 in lateral cell contacts (arrows in detail, D), but not vice versa (E). WiDr (D) and HEK293 (E) cells were transiently transfected with CD97(EGF125) pcDNA3.1 and SAP97-myc pcDNA3.1, respectively, and stained with $CD97^{Cterm}$ and DLG1 Abs.

(F) Pull-down experiments using GST or DLG1-GST and 6-FAM-coupled peptides corresponding to the last 25 amino acids of CD97. The peptides terminated with the non-phosphorylated PBM ASESGI, a mutated ASEAGG, or ASESGI with phosphoserines (in red). Upper: CD97 peptides were stained in a 16% tricine gel with Coomassie brilliant blue. The eluted GST and DLG1-GST were detected by western blot analysis. Modifications such as amino acid replacements (phosphorylation) affect the accessibility for SDS, resulting in gel migration shifts that are proportionately larger for small peptides. Lower: in parallel, the eluted CD97 peptides were quantified by high-performance liquid chromatography (HPLC).

RESULTS

CD97 Interacts with the Scaffold Protein DLG1

CD97 localizes to adherens junctions (Becker et al., 2010). To detect CD97 interaction partners in these contacts, proximity ligation assays (PLAs) were performed. In addition to E-cadherin and β-catenin, CD97 interacted with the scaffold protein DLG1 in DLD1 cells (Figure 1B). This interaction was consistently restricted to lateral cell contacts in human enterocytes (Figure 1C). A transient increase of CD97 in WiDr (Figure 1D) and other cell lines (data not shown) led to CD97 localization in lateral cell contacts and to a concomitant enrichment of endogenous DLG1, implying that CD97 recruits DLG1. However, DLG1 did not enrich CD97 (Figure 1E).

To verify whether CD97 bound to DLG1, DLG1-glutathione S-transferase (GST) pull-down experiments were performed with lysates of HT1080 cells stably overexpressing the shortest isoform of CD97 with three EGF-like domains, CD97(EFG125) (Figure S1A). Western blot analyses of the eluted proteins with CD97 NTF- and CTF-specific antibodies (Abs) showed bands at 74 and 26 kDa. Lysates of cells expressing a C-terminal- to two-span transmembrane (2TM) helix-truncated CD97(EFG125) showed no binding, indicating that DLG1 interacts with the second or third intracellular loop or the ICD of CD97. Pull-downs with several DLG1 deletion mutants revealed binding of CD97 to PDZ domain 1 (PDZ1) and probably to PDZ domain 2 (PDZ2) of DLG1 (Figures S1B and S1C).

Phosphorylation of the PBM of CD97 Disrupts Binding to DLG1

Because phosphorylation at the PBM often regulates binding to PDZ domains (Lee and Zheng, 2010), we repeated pull-down experiments using CD97 peptides with the C-terminal PBM ASESGI (Figure 1F). Binding to DLG1 was disrupted if either or both serines, corresponding to the positions S738 and S740 in the shortest CD97(EGF125) isoform, were phosphorylated. To study the conditions under which CD97 becomes phosphorylated, Abs were generated to phosphorylation of CD97 at S740 (pCD97 S740) and to non-phosphorylated PBM ($CD97^{Cterm}$) Abs (Figures 1A and S1D–S1G).

pCD97 S740 Is Rapidly Induced by Mechanical Stimuli

Because aGPCRs are potential mechanoreceptors, we studied whether mechanical force, applied in a wounding assay or as shear stress induced pCD97 S740 in HT1080 CD97(EFG125) cells. S740 was not phosphorylated without treatment. After scratching, pCD97 S740 was induced within 30 s and began to decrease in less than 10 min in cells at the wound rim (Figure 2A), whereas the level of $CD97^{NTF}$ remained nearly unchanged.

Shear stress induced pCD97 S740 in stressed cellular junctions, retracting fibers of around 0.2 μm in width (Figures 2B and 2C), and in the area where the cells adhered to the dish (data not shown). pCD97 S740-positive retracting fibers were filamentous actin (F-actin) negative in their distal parts (Figure 2C). Consistent with this, pCD97 S740 appeared in the cytosol of still completely attached shear-stressed cells in areas where F-actin had partly vanished (Figure 2D), suggesting that pCD97 S740 occurred in parallel with altered F-actin dynamics. $CD97^{NTF}$ was uniformly distributed.

Moreover, we detected pCD97 S740 *in vivo* by immunostaining tissues containing strongly CD97-positive cells such as scattered colorectal tumor cells and leukocytes (Figure S2). As *in vitro*, the CD97 NTF was still present in pCD97 S740-positive cells.

pCD97 S740-Positive Membrane Patches Indicate Cytosolic Dissociation of Cellular Adhesion

Retracting or detached shear-stressed cells left membrane patches of 0.60 ± 0.05 μm (n = 30) in diameter at the location from which the cells were displaced (Figures 2E and 2F). These footprints were stained for pCD97 S740 and the focal adhesion contact protein β1-integrin (CD29). The presence of the CD97 C terminus in the patches revealed that the cells detached at their cytosolic interface, suggesting that PBM phosphorylation disrupts CD97 binding to intracellular proteins, as demonstrated for DLG1 in pull-down experiments. The CD97 NTF was also present in these membrane patches, indicating that S740 phosphorylation led to neither extracellular detachment at the autocatalytic GPS nor complete NTF shedding or internalization.

The PBM Is Critical for CD97-Modulated Detachment and Mechanical Cellular Properties

To verify whether the PBM is critical for the intracellular anchoring of CD97, we compared the reaction under shear stress, the mechanical properties, and the actin structure of HT1080 CD97(EGF125) cells with HT1080 cells expressing CD97(EGF125) but lacking the PBM (ΔPBM) (Figure 3). Although both cell types had comparable CD97 surface levels (Figure 3A), shear-stressed ΔPBM cells retracted and lost cell-cell contacts faster (Figure 3B). Because the composition and intracellular anchorage of the cytoskeleton determine cellular viscoelastic properties, we probed their dependence upon the PBM in an optical stretcher. ΔPBM cells showed higher maximum relative deformability (Figure 3C), which measures the contribution of cytoskeletal filaments to mechanical properties. Consistently, after seeding, ΔPBM cells remained rounded longer (data not shown), thus adhering less to the dish (Figure 3D).

Membrane Localization of CD97 Depends on Cortical F-Actin

The data indicate that the PBM links CD97 to the cytoskeleton. CD97 and the F-actin cortex co-localized well (Figure 3E). Treatment of the cells with cytochalasin D, blocking the polymerization and elongation of F-actin, disrupted the membrane localization of CD97. Consistently, the actin structure differed between shear-stressed HT1080 CD97(EGF125) and ΔPBM cells (Figure 3F), although the ratio between filamentous and globular actin (F/G-actin) was comparable in untreated cells (Figure 3G).

CD97 Knockout Partly Phenocopies CD97(EGF125) ΔPBM

If the PBM anchors CD97 intracellularly to the cytoskeleton, cells lacking CD97 might partly phenocopy the viscoelastic properties of ΔPBM cells. To verify this assumption, we investigated MDA-MB-231 cells with high endogenous CD97. In these cells, shear stress also induced pCD97 S740-positive retracting fibers (Figure S3A). We applied a CRISPR-Cas9 approach to prevent CD97 expression (Figure S3B). MDA-MB-231 CD97 knockout (KO) clones partly behaved like CD97(EGF125)ΔPBM cells, especially in cellular properties influenced by the actin cytoskeleton, such as spreading after seeding and relative deformability (Figures S3C and S3D). Partly non-stressed CD97KO clones already showed an altered actin structure and F/G-actin ratio (Figures S3E and S3F) and slight alterations in key proteins of the LIM kinase (LIMK)/cofilin pathway, which regulates actin filament dynamics, compared to MDA-MB-231 wild-type (WT) cells (Figure S3G).

Protein Kinases with a Phorbol Ester and DAG-Responsive C1 Domain Can Phosphorylate CD97 S740

To identify kinases that could potentially be responsible for phosphorylating S740 in the wounding assay, we pre-incubated HT1080 CD97(EFG125) cells with various kinase inhibitors. The use of 50 nM staurosporin, a protein kinase C (PKC) and protein kinase D (PKD) inhibitor with poor specificity, was able to inhibit S740 phosphorylation (Figure 4A). In addition, pCD97 S740 induction upon wounding was partly inhibited by preincubation with 10 μM bisidolylmaleimide I hydrochloride (BIM I), a PKC inhibitor with selectivity for PKC α, β1, β2, γ, δ, and ε isozymes, or with 100 μM CID755673, a PKD inhibitor that, at higher concentration, also blocks PKCs. The protein kinase A (PKA) inhibitor H89, the casein kinase 2 (CK2) inhibitor III, and paroxetine, the only available specific inhibitor of a GPCR-related kinase (GRK), were ineffective.

The classic (α, β1, β2, and γ isozymes) and novel PKCs (δ, ε, η, and θ isozymes), as well as PKD1–PKD3, all of which are

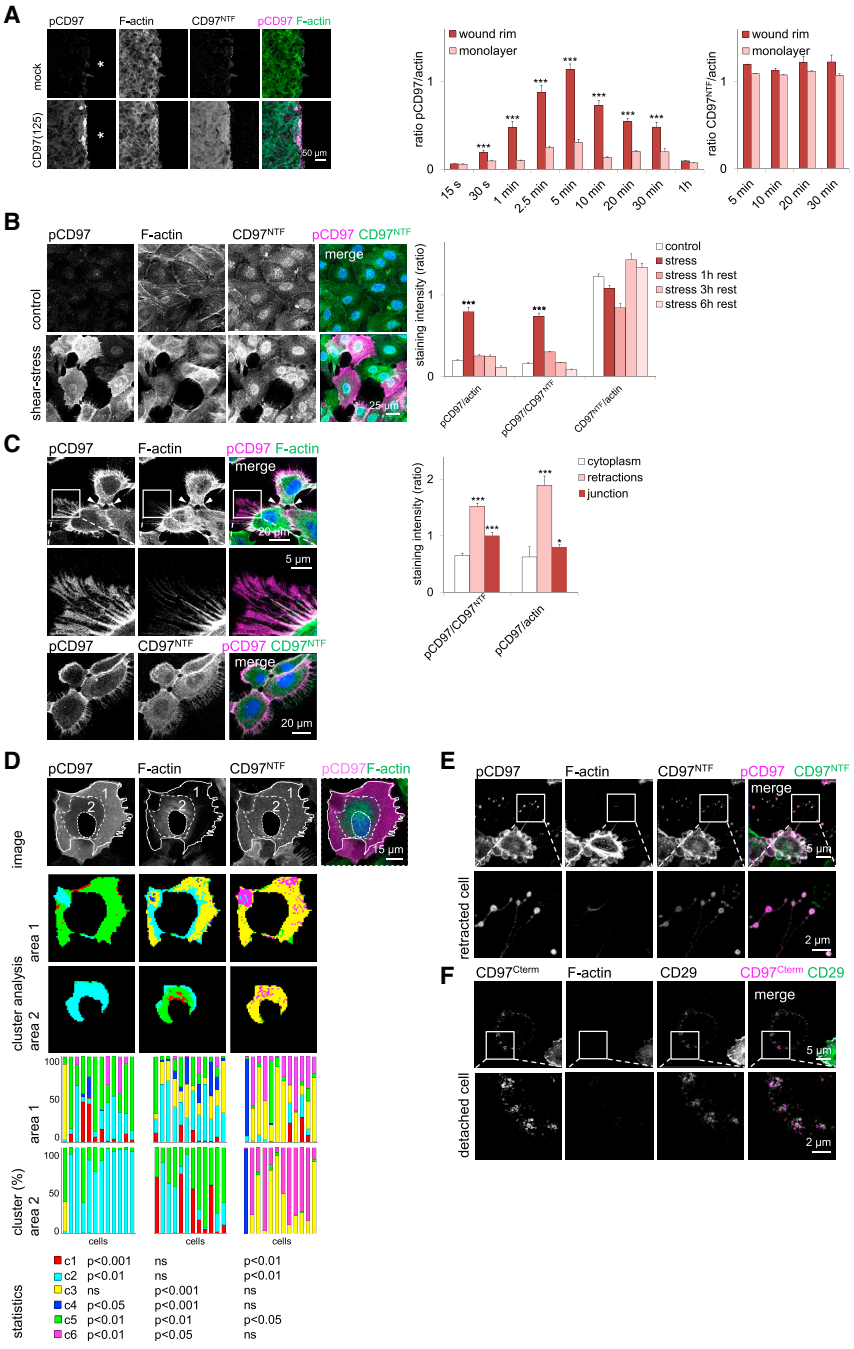

Figure 2. Mechanical Force Rapidly Induces pCD97 S740

(A) HT1080 CD97(EGF125) cells were pCD97 S740 negative in the absence of stimuli. Left: wounding (*) of the monolayer induced pCD97 S740 in cells at the wound rim. This was not the case in mock-wounded cells. The cells were co-stained for pCD97, CD97^{NTF}, and F-actin. Right: ratios of the staining intensities were quantified in cells either at the wound rim or within the monolayer; time after wounding is indicated. n = 10 optical fields, mean ± SEM; ***p < 0.001 rim compared with the monolayer.

(B) Left: HT1080 CD97(EGF125) cells were shear stressed (20 dyn/cm^2; 12 min) and co-stained for pCD97 S740, CD97^{NTF}, and F-actin. Right: staining intensities were quantified before, immediately after, and 1, 3, and 6 hr after shear stress. n = 10 optical fields, mean ± SEM; ***p < 0.001 compared with control.

(C) pCD97 S740 was induced in stressed junctions (arrows) and retracting fibers (detail) of shear-stressed HT1080 CD97(EGF125) cells (20 dyn/cm^2, 6 min). The cells were co-stained for pCD97 S740, CD97^{NTF}, and F-actin, and ratios of the staining intensities, measured 1 µm from the dish bottom, were determined for the various cellular compartments. n = 10 cells, mean ± SEM; **p < 0.01, ***p < 0.001 compared with cytoplasm. F-actin was not present in the distal parts of retracting fibers.

(D) pCD97 S740 induction paralleled F-actin turnover. Upper: shear-stressed HT1080 CD97(125) cells (20 dyn/cm^2, 12 min) were co-stained for pCD97 S740, CD97^{NTF}, and F-actin; one typical cell is shown. Actin and CD97^{NTF} structures were analyzed in still completely attached cells in their pCD97 S740-positive areas (1) and S740-negative areas (2) (Möller et al., 2014). The nucleus and areas in which cells overlapped were excluded from analyses. Middle: in the correspondingly labeled images of areas 1 and 2, each tile color refers to a cluster ID. Six clusters were applied. Lower: cell-wise pCD97, F-actin, and CD97^{NTF} cluster distribution; each bar refers to a single cell. Whereas the F-actin clusters were different between the pCD97 S740-positive area (1) and the S740-negative area (2), the main CD97^{NTF} clusters (c2 and c6) were equally distributed. n = 12 cells, comparison between area 1 and 2. ns, not significant.

(E and F) Membrane patches were lost at the dish from shear-stressed rounded (E) and detached (F) HT1080 CD97(125) cells (20 dyn/cm^2, 20 min). The patches (details) were pCD97 S740, CD97^{NTF}, CD97^{Cterm}, and β1-integrin (CD29) positive but lacked F-actin.

kinases with a phorbol ester and diacylglycerol (DAG)-responsive C1 domain, can be activated by DAG. Consistently, 10 ng/mL phorbol 12-myristate 13-acetate (PMA) (Figures 4C and 4D) and 100 µM membrane-permeable 1-oleoyl-2-acetyl-sn-glycerol (OAG) (data not shown), both of which mimic DAG activity, were able to induce pCD97 S740, as did 2 nM bryostatin 1, a potent activator of PKC and PKD (data not shown). Western blot analysis confirmed that S740 was phosphorylated in the presence of PMA and that, in parallel, the CD97 NTF was still present (Figure 4C). We were able to block PMA and shear stress-induced pCD97 S740 only by application of staurosporin (Figures 4C and 4D), indicating that several PKC/PKDs can phosphorylate CD97 at S740 under this condition.

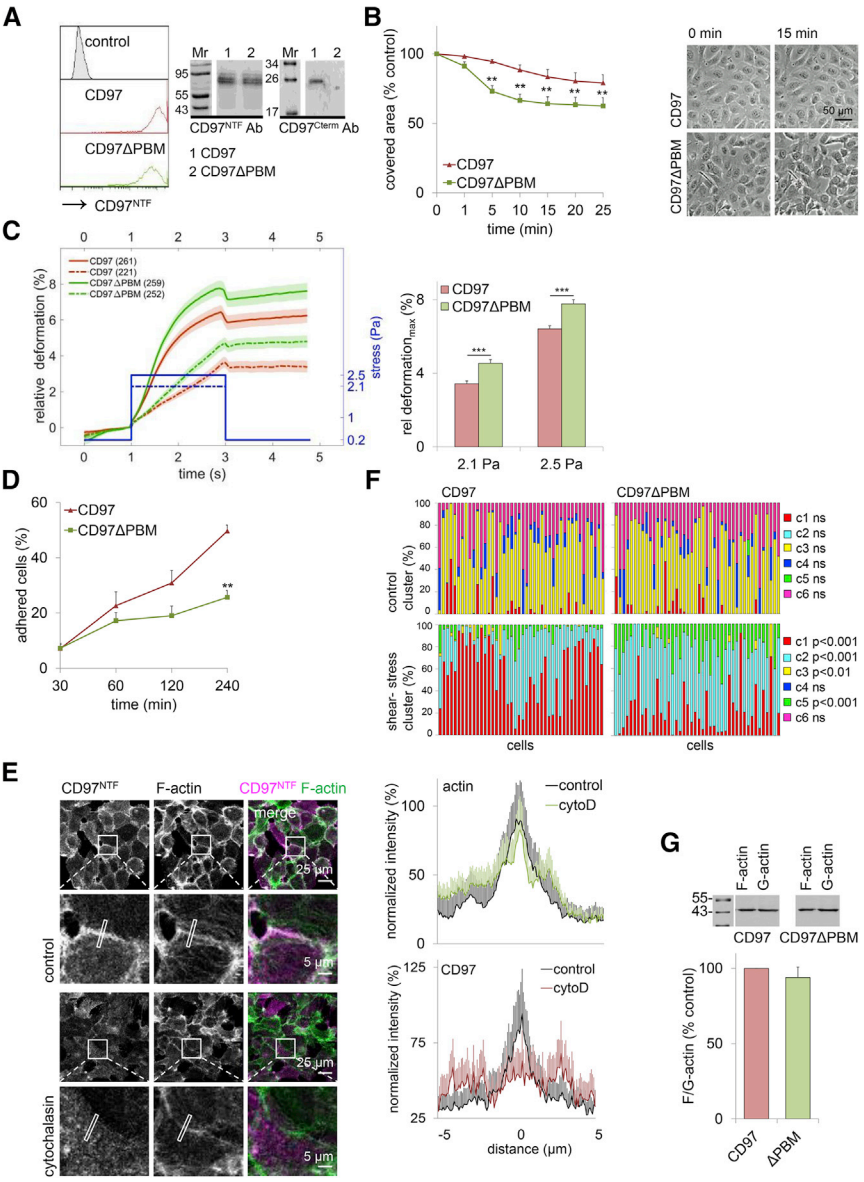

Figure 3. Deletion of the PBM in CD97 (EGF125) Alters the Cellular Properties

(A) Left: HT1080 CD97(EGF125) and CD97 (EGF125)ΔPBM cells expressed similar levels of CD97 at the surface, as shown by flow cytometry with the CD97^{NTF} Ab. Right: western blot analysis with the CD97^{Cterm} Ab revealed the absence of the PBM in lysates of CD97(EGF125)ΔPBM cells; Mr, molecular weight marker.

(B) Densely cultured HT1080 CD97(EGF125) and CD97(EGF125)ΔPBM cells were subjected to shear stress (20 dyn/cm^2). Left: cell-covered area quantified over time in bright-field images. n = 5 experiments, n = 6 optical fields/experiment, mean ± SEM; **p < 0.01 compared with CD97(EGF125). Right: typical images taken at the beginning and after 15 min of shear-stress application.

(C) Analysis of relative deformability of HT1080 CD97(EGF125) and CD97(EGF125)ΔPBM cells in an optical stretcher. Left: mean and 95% confidence interval. The applied laser pattern is indicated by the blue line: cells were trapped for 1 s, and then 2.1 Pa (dotted line) or 2.5 Pa (solid line) stress was applied for 2 s, followed by 2 s additional trapping. The numbers of analyzed cells are indicated in brackets. Right: maximal relative deformation at 2.1 and 2.5 Pa, mean ± SEM. ***p < 0.001 compared with CD97(EGF125).

(D) 4 × 10^3 HT1080 CD97(EGF125) or CD97(EGF125)ΔPBM cells were seeded to a 96-well, and the number of adherent cells was quantified after attachment in bright-field images taken before and after washing the wells. n = 5 experiments, n = 3 wells/experiment, mean ± SEM; **p < 0.01 compared with CD97(EGF125).

(E) Left: in HT1080 CD97(125) cells, CD97 co-localized well with cortical F-actin at the lateral junctions. Cytochalasin D (cytoD) delocalized junctional CD97. Cells were stained for CD97^{NTF} and F-actin before and after treatment with 1 µM cytochalasin D for 4 min; details: the distribution of CD97 and F-actin was quantified at the indicated location. Right: the distribution of CD97 and F-actin was quantified in plot profiles of 10 µm across the junctions. n = 10 junctions, 0 = junctional midpoint, mean ± SEM.

(F) Under shear stress (20 dyn/cm^2, 10 min), actin organization was altered in HT1080 CD97(EGF125)ΔPBM compared with CD97(EGF125) cells. Actin cluster analysis of untreated and shear-stressed cells is shown. Statistics of the six applied actin clusters (c1–c6) were collected. n = 50 cells/cell type/condition. NS, not significant.

(G) F/G-actin ratio showed no difference between untreated HT1080 CD97(EGF125) and CD97(EGF125)ΔPBM cells. Upper: one typical experiment is shown. Lower: n = 5, mean ± SEM.

Finally, we investigated the possibility of phosphorylation of CD97 S740 by PKC/PKD activation by sensing the mechanical stimuli by a non-CD97 GPCR. However, YM-254890, a GNAQ/11-selective inhibitor, did not inhibit pCD97 S740 induction in the wounding assay (data not shown).

PBM- and GNA12/13-Mediated Signaling of CD97 Are Partly Independent

Up to this point, we have demonstrated that CD97 shapes the mechanoresponse of cells. The question that remains is: does CD97 sense mechanical stimuli leading to pCD97 S740 induction?

By analyzing second messenger production, we have confirmed the presence of a tethered agonistic sequence, the so-called *Stachel* (Figure 1A) (Liebscher et al., 2014; Stoveken et al., 2015), based on mutants lacking the NTF (ΔNTF) or lacking the complete ECD (ΔECD) (Figures 5A–5E). Only serum response element (SRE) levels were significantly increased through the expression of the constitutively active mutant ΔNTF. Deletion of the N-terminal-remaining amino acids up to the first transmembrane domain (ΔECD) or just the first six *Stachel* amino acids (S438_L443del) of this mutant abrogated the SRE signal. Unfortunately, HT1080 cells expressing CD97(EGF125)

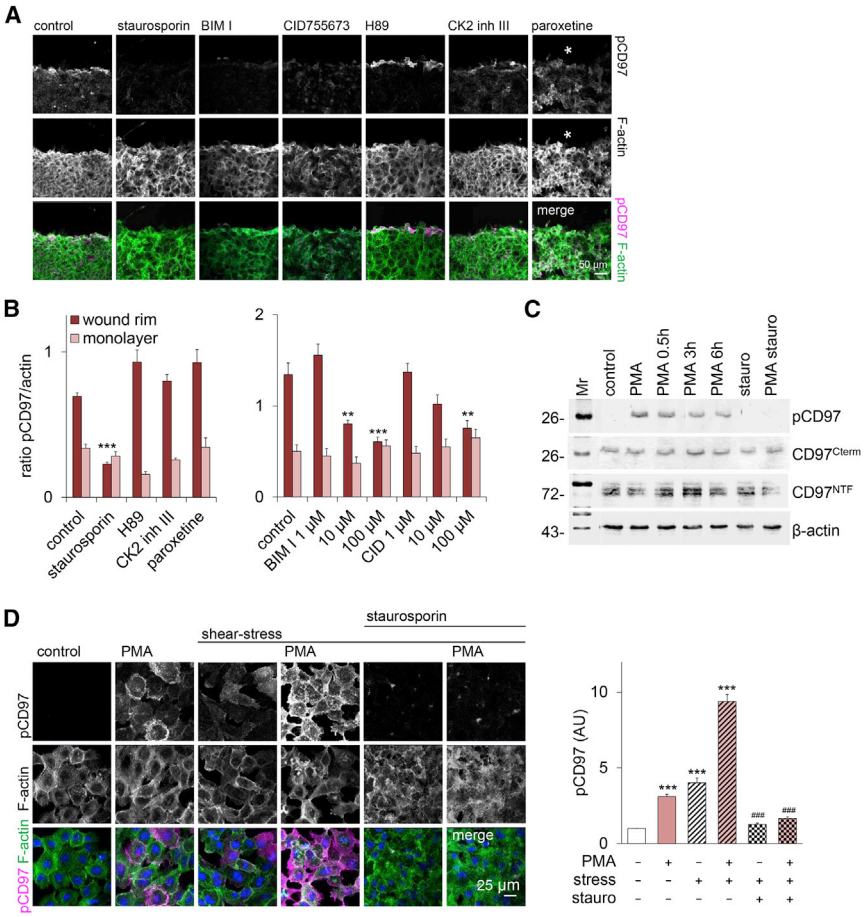

Figure 4. Protein Kinases with a Phorbol Ester and DAG-Responsive C1 Domain Can Phosphorylate CD97 S740

(A and B) pCD97 S740 induction was strongly inhibited by staurosporin in the wounding assay. (A) Confluent HT1080 CD97(EGF125) cells were pre-incubated for 60 min with 50 nM staurosporin, 10 μM BIM I, 100 μM CID755673, 1 μM CK2 inhibitor III, 5 μM H89, and 200 μM paroxetine before wounding (*). 6 min after wounding, the cells were stained for pCD97 S740 and F-actin. (B) pCD97 S740 and actin staining was quantified in the cells at the wound rim and cells within the untouched monolayer. n = 10 optical fields, mean ± SEM; $^{**}p < 0.01$, $^{***}p < 0.001$ to control.

(C) Phosphorylation of CD97 S740 did not result in shedding or degradation of the CD97 NTF or CTF, respectively. HT1080 CD97(EGF125) cells were treated with 10 ng/mL PMA, 500 nM staurosporin (stauro), or both for 10 min. When PMA was applied alone, it was removed after 10 min and cells were incubated with medium for a further 0.5, 1, and 3 hr. Western blot analysis of the lysates with the indicated Abs. Mr, molecular weight marker.

(D) PMA and shear stress-induced pCD97 S740 was inhibited by staurosporin. Left: HT1080 CD97(EGF125) cells were pre-treated with 10 mg/mL PMA (10 min), 500 nM staurosporin (50 min), or both before the application of shear stress (20 dyn/cm^2, 5 min). Right: pCD97 S740 was quantified in microscopic pictures. n = 10 optical fields, mean ± SEM; $^{***}p < 0.001$ compared with control, $^{###}p < 0.001$ compared with PMA-treated and shear-stressed cells.

S438_L443del failed to grow, and the application of derived synthetic peptides in second messenger and cellular assays was hampered by their very low solubility. Applying direct mechanical force such as vibration or shaking to CD97(EGF125)-transfected cells did not increase the SRE level (Figure 5C), which was in line with the fast time frame of the CD97-dependent mechanoresponse mediated by its PBM. Furthermore, mechanical challenges did not induce signaling via cyclic AMP (cAMP) and inositol triphosphate (IP3). Thus, we have identified the CD97 agonistic sequence, but it remains unknown whether it is the CD97 sensor of mechanical force.

Interestingly, the SRE signal was decreased not by deleting the PBM (ΔPBM) but by deleting the ICD up to the last nine amino acids (V701_R733del) in the active ΔNTF mutant (Figures 5D and 5E). ΔNTF V701_R733del was able to induce pCD97 S740 (data not shown). Consequently, we can say that PBM- and GNA12/13-mediated signaling of CD97 are (partly) independent.

Finally, we have verified that the ECD length may adjust an aGPCR response toward mechanical challenges, as was shown for the *Drosophila* aGPCR dCirl (Scholz et al., 2017). Autoproteolytic processing at the GPS inside the ECD was not necessary for dCirl-dependent mechanosensation but may be relevant for other aGPCRs. Here, we show that shortening of the CD97 extracellular region by deleting the EGF-like folds (ΔEGF) and prevention of CD97 cleavage in two CD97(EGF125) mutants, H436S and S438G, did not prevent pCD97 S740 induction (Figure 5F). CD97ΔEGF appeared only partly at the cell surface, which rendered further testing of its influence on biomechanical cellular properties impossible.

DISCUSSION

Here, we have demonstrated that an aGPCR transduces mechanical force via its C-terminal PBM into a cellular response. Phosphorylation of the CD97 PBM at S740, triggered by various mechanical stimuli, probably regulates the intracellular binding of this receptor. pCD97 S740 induction is of physiological and pathophysiological relevance: we detected pCD97 S740 *in vivo* in subpopulations of CD97-positive tumor cells and leukocytes, i.e., cells that dissociate from other cells or from the extracellular matrix during migration and invasion.

Conspicuously, in cells with endogenous or heterologous CD97 expression, pCD97 S740 was induced at stressed cellular junctions, in retracting fibers, and in the detachment area *in vitro*. Retracting or detaching cells leave membrane patches containing the S740 phosphorylated CTF of CD97. Generally, cells detach at the weakest protein-protein interface; either the rupture occurs at the extracellular site, usually between the

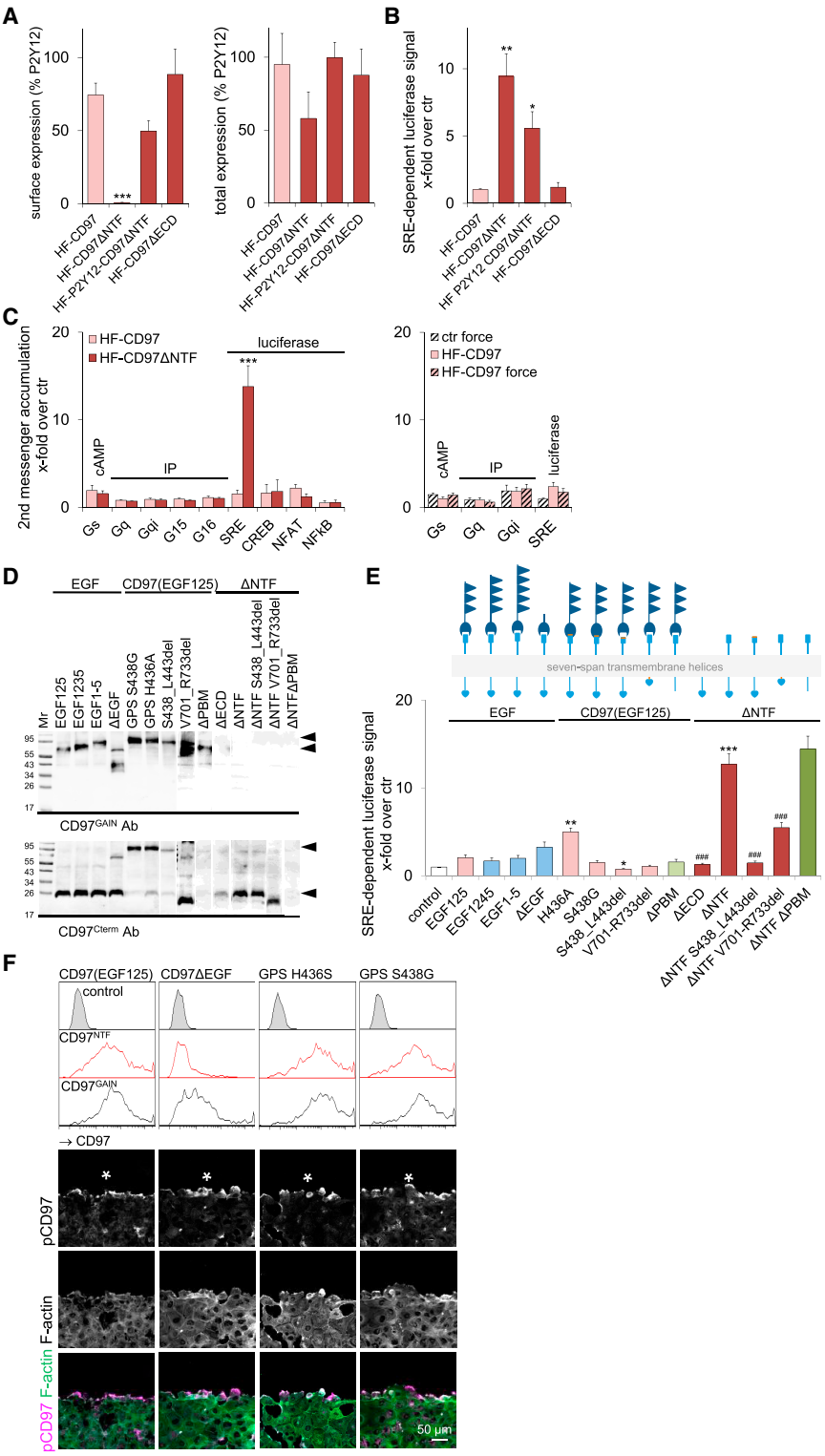

Figure 5. Determinants of CD97 G Protein- and PBM-Dependent Signal Transduction

(A) To compare cell surface and cellular expression, Cos-7 cells were transfected with N-terminally (hemagglutinin [HA]) and C-terminally (FLAG) tagged full-length CD97(EGF125) and truncated ΔNTF constructs, as well as a fusion ΔNTF construct with an added N terminus of $P2Y_{12}$ (Liebscher et al., 2014) in a pcDps backbone. Left: cell surface expression of the HA tag was monitored. Right: to assess the total cellular amounts of full-length HA/FLAG the double-tagged constructs, a sandwich ELISA was performed (Römpler et al., 2006). Optical density (OD) values are given as the percentage of human $P2Y_{12}$, which served as a positive control. Although CD97(EGF125) and the ΔECD mutant are well expressed at the cell surface, the truncated ΔNTF mutant was only detectable when fused to the N terminus of $P2Y_{12}$. Total cell expression is detectable for all displayed constructs, indicating proper protein maturation.

(B) To functionally evaluate the results from the cell surface expression analysis for the receptor mutants, we applied a previously reported readout for CD97 activation, which uses a serum response element (SRE) luciferase signal that should increase upon deletion of the NTF (Ward et al., 2011). Both receptor mutants displayed significant increase in signaling activity compared to the full-length receptor CD97(EGF125), indicating that the non-surface-detectable ΔNTF construct is a functional protein. However, the mutant lacking the complete ECD shows no signaling activity besides WT-equivalent surface and total cell expression, pointing to the importance of the putative *Stachel* sequence for this signal transduction pathway.

(A and B) n = 5 independent experiments, mean ± SEM; *p < 0.05, **p < 0.01, ***p < 0.001 compared with full-length CD97 (EGF125).

(C) To verify Gα protein coupling of CD97, cells were transfected with CD97(EGF125) and CD97ΔNTF constructs and an array of second messengers was tested for a change in signaling levels. Left: significant activation for the CD97ΔNTF mutant was only seen in the SRE assay. Right: application of vibration at 17 Hz did not change signaling levels. Results are given as x-fold over empty vector control (ctr). n = 5 independent experiments, mean ± SEM; ***p < 0.001 compared with control.

(D) To perform detailed structure-function analysis of CD97 in the SRE assay, new mutants were generated and verified by western blot analysis of Cos-7 cells transiently transfected with the various constructs. Because C-terminal tags prevent binding of the pCD97 S740 and $CD97^{Cterm}$ Abs and likely phosphorylation at the PBM, and because N-terminal tags at the ΔNTF mutants may disturb the functionality of the predicted agonistic *Stachel* sequence, we used CD97 expression constructs in a pcDNA3.1 backbone without tags. The polyclonal $CD97^{GAIN}$ and $CD97^{Cterm}$ Abs were applied to detect cleaved CD97 with its NTF and CTF (~26 kDa), respectively. The NTF size depends on the number of EGF-like domains and on the degree of N glycosylation (Wobus et al., 2004). The arrows indicate cleaved and uncleaved CD97(EGF125). The mutant lacking the EGF-like folds (ΔEGF) showed the truncated NTF, and the mutants lacking the ICD up to the last nine amino acids (V701_R733del) showed the truncated CTF. We generated two mutants with a non-cleavable GPCR proteolysis site (GPS): H436A and S438G. In H436A amino acid −2 relative to the GPS and in S438G amino acid +1 of the predicted *Stachel* were mutated, respectively. Both positions are conserved and

(legend continued on next page)

substrate and the transmembrane receptor, or it occurs at an interface inside the cell, which could be mediated by phosphorylation of the transmembrane receptor or of their intracellular adaptor proteins and binding partners (Kirfel et al., 2004; Sun et al., 2016). Consequently, detachment of cells at their cytosolic interface results in a loss of cell material, as we observed for the pCD97 S740, CD97^{NTF}, and β1-integrin (CD29)-positive membrane patches. The footprint phenomenon is well known in the rear detachment of migrating cells, as integrin-containing cellular material is left behind them, forming characteristic migration tracks that mark the direction the cell has taken (Kirfel et al., 2004). Unlocking cell contacts inside the cell between CD97 PBM and intracellular proteins releases attachment and may prevent cell injury. Perhaps phosphorylation determines the threshold of forces transmitted inside the cell and terminates the junctional function of CD97. Phosphorylation at the PBM subsequently may permit binding to other intracellular proteins, such as members of the 14-3-3 family, as has been shown for the human papillomavirus E6 oncoprotein (Boon and Banks, 2013).

The CD97 NTF is also present in such lost patches, suggesting that detachment does not occur extracellularly at the GPS at which CD97 is almost always cleaved. Thus, the CD97 NTF and CTF partly remained non-covalently associated under shear stress, and rupture of PBM binding did not result in complete shedding or internalization of the NTF or degradation of the CTF. Consistently, the presence of paroxetine, a specific inhibitor of a GRK that phosphorylates activated receptors and promotes arrestin binding, thus precluding further G protein coupling and inducing internalization of the receptor, was not able to inhibit pCD97 S740 induction.

The aGPCR CD97 is part of the junctional signaling complex consisting of E-cadherin, catenins, and scaffold proteins such as DLG1, which together are linked to the F-actin cortex (Takeichi, 2014). The ability of adherens junctions to withstand mechanical forces critically depends on its connection to F-actin (Mattila et al., 2016). CD97 strengthens adherens junctions of intestinal epithelial cells of Tg(villin-CD97) mice in an experimental colitis model (Becker et al., 2010). Ultrastructural pictures feature condensed cytoskeletal elements at these junctions (Becker et al., 2010), suggesting that CD97 modulates the actin cytoskeleton and/or its linkage to the cell membrane. We confirmed this hypothesis through several cellular approaches in which CD97 S740 phosphorylation was mimicked by deletion of the PBM, indicating disruption of PBM binding to intracellular proteins. HT1080 CD97(EGF125)ΔPBM cells showed an increased relative deformability during optical cell stretching; they remained rounded and took longer to adhere after seeding. Under shear stress, they lost cell contacts faster and had an altered actin structure compared with cells expressing the full-length receptor. CD97 KO in MDA-MB-231 cells, which express high endogenous levels of CD97, partly phenocopies these alterations: the relative deformability and F-actin structure were altered in cells without CD97. Of all cytoskeletal filaments, F-actin makes the largest contribution to cellular stiffness and determines the elastic cell response at relatively low strain rates in an optical stretcher (Gladilin et al., 2014; Kubitschke et al., 2017). Accordingly, the cell softening seen after deletion of the PBM or CD97 KO can be attributed to a reduction of the effective density and stiffness of actin filament networks. Cytochalasin-D-treated F-actin-deficient NK-21-C1 cells exhibit 41% greater deformability, in comparison with the untreated control cells (Gladilin et al., 2014).

CD97 is organized at the membrane in a F-actin cortex-dependent manner. Cytochalasin D not only destabilized the F-actin cortex but also dramatically disturbed the localization of junctional CD97 in cells with endogenous or heterologous CD97. The interaction of CD97 and the F-actin cortex is probably indirect (the CD97 ICD does not contain a putative actin-binding site), suggesting that other molecules may mediate the communication between CD97 and F-actin. Here, we have identified DLG1, an intracellular CD97 ligand with three PDZ domains, as one potential candidate for this molecular bridge, although this remains to be formally demonstrated *in vivo*.

Our data make evident that CD97 shapes the cellular mechanoresponse by modulating binding at its PBM. The interaction of PBMs with PDZ domains is almost always turned off by dephosphorylation of serine, threonine, or tyrosine in the p(−2) site of the PBM, a result of the elimination of an essential hydrogen bond donor side chain (Lee and Zheng, 2010). We identified PKC and PKD, both known to contribute to the mechanical force-induced cellular responses (Sivaramakrishnan et al., 2009;

necessary for cleavage (Lin et al., 2004). The mutant lacking the first six amino acids of the proposed agonistic sequence (S438_L443del) was also mostly uncleaved.

(E) Structure-function analysis was performed using differences in basal signaling activities in the SRE assay as readout and the various CD97 isoforms and mutants. Upper: schema of the CD97 isoforms and mutants (see also D and Figure 1A). Either the number of EGF-like folds was different (CD97 isoforms and a mutant lacking the EGF-like folds) or the CD97 isoform with three EGF-like folds (EGF125) was mutated. Mutants lacking at least the NTF are shown on the right. Lower: SRE assay was assigned to the CD97 isoforms and mutants in the upper panel. These data stress the possibility of the presence of a tethered agonistic sequence within CD97, because again, mutants lacking the complete ECD (ΔECD) or just the first six amino acids of the predicted agonistic sequence (S438_L443del) stopped signaling activity of CD97ΔNTF. Signaling without the *Stachel* sequence can be possible (Kishore et al., 2016; Salzman et al., 2016, 2017), but we saw no indication for this in any assay we tested. Deletion of the ICD up to the last nine amino acids (V701_R733del) of the ΔNTF mutant decreased the SRE signal obviously, whereas deletion of the PBM (ΔPBM) had no effect. The number or presence of EGF-like folds did not alter the basal activity of CD97. Results are given as x-fold over empty vector control; mean ± SEM. n = 8 independent experiments; *p < 0.05, **p < 0.01, ***p < 0.001 compared with CD97(EGF125), ###p < 0.001 compared with CD97ΔNTF.

(F) EGF-like folds and autoproteolytic processing in the extracellular domain are dispensable for pCD97 S740 induction. EGF-like folds anchor CD97 to CD55 and integrins (Hamann et al., 1996; Wang et al., 2005) or to an extracellular matrix constituent (Stacey et al., 2003). To test the role of cleavage at CD97 S740 phosphorylation, we prevented autoproteolytic activity in the H436G and S738A mutants (Figure 5D). Upper: cell surface expression of the HT1080 CD97 mutant cell lines examined by flow cytometry using the CD97^{NTF} Ab, which binds to the EGF-like folds, and the monoclonal CD97^{GAIN} Ab, which binds within the GAIN domain. CD97ΔEGF appeared only partly at the cell surface, which rendered further testing of its influence on biomechanical cellular properties impossible. Lower: wounding of monolayers of these HT1080 CD97 mutant cell lines induced pCD97 S740 in cells at the wound rim. Cells were co-stained for pCD97 S740 and F-actin.

Yang et al., 2013), as candidates to phosphorylate CD97 at S740. PKC α interacts, via its PBM, with the third PDZ domain of DLG1 (O'Neill et al., 2011), the intracellular CD97 interaction partner identified here.

Mechanical force activates kinases that then can phosphorylate the CD97 PBM, which leads to the question of whether the mechanical stimulus is sensed by CD97. Switch-like models divide mechanotransduction, the conversion of mechanical forces into biochemically relevant information (such as CD97 phosphorylation at its PBM), into mechanotransmission, mechanoreception, and mechanoresponse (Hoffman et al., 2011). The force must be transmitted to a mechanosensitive structure, which responds by altering its conformation. The new conformation can then trigger signaling networks that need not be specifically force dependent.

By examining CD97 Gα protein coupling, we have here identified the CD97 agonistic *Stachel*, a putative mechanosensitive structure aGPCR (Liebscher et al., 2014; Petersen et al., 2015; Stoveken et al., 2015; Wilde et al., 2016). However, none of the second messenger assays we performed showed activation through mechanical force. Most likely, the time frame of the CD97 mechanoresponse is too short to be detected in accumulation assays, yet real-time signaling approaches require the additional transfection of the given sensors, which also interferes with the fast CD97 mechanoresponse. CD97 binds only to GNA12/13, even in mechanically challenged cells, indicating signaling to the small guanosine triphosphatase (GTPase) RHOA, which promotes formation of actomyosin contractile arrays via its key effector proteins: formin, leading to unbranched actin polymerization, and ROCK, which activates myosin. Instead, CD97 signaling via PBM phosphorylation causes F-actin depolymerization, which results in an enhanced detachment. Consistently, GNA12/13 coupling and PBM phosphorylation are facilitated by different parts of the CD97 ICD. We have also demonstrated that alterations of the CD97 extracellular region, suggested to be responsible for increasing the tension of aGPCRs (Scholz et al., 2017) by shortening and prevention of CD97 cleavage, did not inhibit pCD97 S740 induction.

Scenarios in which proteins other than CD97 sense the mechanical force are also conceivable. CD97 localizes to adherens junctions, a mechanosensitive unit. Several of its structural components may transmit and/or sense mechanical stimuli. The junctional stability is, for example, determined by conformational changes in proteins linking the cell surface receptor E-cadherin to the cytoskeleton, such as α-actinin and vinculin, or regulated in an inside-outside fashion through alterations of the actomyosin apparatus (Yonemura et al., 2010; Takeichi, 2014). E-cadherin, another potential CD97 interaction partner identified in the PLA, facilitates PKD1 plasma membrane translocation and activation (Li et al., 2016). Membrane-localized PKD1 can be activated in the absence of DAG (Li et al., 2016); this could explain why the GNAQ/11-selective inhibitor YM-254890, which would inhibit a mechanosensitive non-CD97 GPCR upstream of CD97, subsequently releasing DAG, did not prevent S740 phosphorylation. However, how CD97 is structurally embedded in, and linked to, this adhesive signaling complex must be clarified in new approaches.

In summary, we report the description and evaluation of a specific phosphorylation site at the PBM of an aGPCR, CD97, that shapes the mechanoresponse of cells bearing this receptor.

EXPERIMENTAL PROCEDURES

Ethics Statement

The Ethics Committee of the Medical Faculty of the University of Leipzig approved the study of human tissues (no. 028/2000 and 111/2009), and all patients gave written informed consent. To immunize rabbits, we obtained an ethics approval from the Landesdirektion Leipzig (V06/14).

Abs

The Abs used in this study are summarized in Table S1. For clarity, the CD97 Abs have been indicated together with their binding site (Figure 1A; Table S1). The generation and validation of the CD97 S740 phospho-specific Ab (S740 of NP_001775.2) is described in detail in Supplemental Experimental Procedures.

Application of Mechanical Forces

For wounding, cells were cultured to confluence and the monolayer was scratched with a pipette tip. For shear-stress experiments, cells were seeded into μ-slides (Ibidi, Munich, Germany), cultured for 48 hr, and subjected to shear stress of 1–20 dyn/cm^2 using the Ibidi pump system. Cells were monitored continuously by confocal laser scanning microscopy. Optical stretcher measurements were described in detail in Supplemental Experimental Procedures.

Image and Statistical Analysis

Ilastik (http://ilastik.org) was used as interactive image classification and segmentation software to quantify the cell-covered area. Staining intensities and the number of attached cells were quantified in images using fiji (http://fiji.sc). Actin structures were analyzed using the fiji plugin MiToBo (Möller et al., 2014). Statistical analyses were performed using SPSS v.24.0 (IBM, Ehningen, Germany). Means ± SEM are given, and the two-side t test was applied if not otherwise stated; p values < 5% were considered significant.

SUPPLEMENTAL INFORMATION

Supplemental Information includes Supplemental Experimental Procedures, three figures, and one table and can be found with this article online at https://doi.org/10.1016/j.celrep.2018.07.071.

ACKNOWLEDGMENTS

The work was supported by grants from the German Research Foundation (DFG) to G.A. (AU 132-7/3 and FOR2149, P08) and I.L. (FOR2149, P05). We thank T. Langenhan and M. Thomas for critical reading of the manuscript, L. Zaenker for analyzing microscopic pictures, and P. Beckmann for cell culture experiments.

AUTHOR CONTRIBUTIONS

G.A., D.H., D.S., F.H., S.R., E.W., M.Q., J.S., L.S., I.L., and N.A.H. conducted the experiments; G.A., S.R., and I.L. designed the experiments; J.A.K. and L.B. provided important resources; L.B. provided substantial corrections of the manuscript; and G.A. wrote the manuscript.

DECLARATION OF INTERESTS

The authors declare no competing interests.

Received: June 22, 2017
Revised: June 5, 2018
Accepted: July 19, 2018
Published: August 21, 2018

REFERENCES

Becker, S., Wandel, E., Wobus, M., Schneider, R., Amasheh, S., Sittig, D., Kerner, C., Naumann, R., Hamann, J., and Aust, G. (2010). Overexpression of CD97 in intestinal epithelial cells of transgenic mice attenuates colitis by strengthening adherens junctions. PLoS ONE *5*, e8507.

Boon, S.S., and Banks, L. (2013). High-risk human papillomavirus E6 oncoproteins interact with 14-3-3ζ in a PDZ binding motif-dependent manner. J. Virol. *87*, 1586–1595.

Boyden, S.E., Desai, A., Cruse, G., Young, M.L., Bolan, H.C., Scott, L.M., Eisch, A.R., Long, R.D., Lee, C.C., Satorius, C.L., et al. (2016). Vibratory urticaria associated with a missense variant in ADGRE2. N. Engl. J. Med. *374*, 656–663.

Gladilin, E., Gonzalez, P., and Eils, R. (2014). Dissecting the contribution of actin and vimentin intermediate filaments to mechanical phenotype of suspended cells using high-throughput deformability measurements and computational modeling. J. Biomech. *47*, 2598–2605.

Hamann, J., Vogel, B., van Schijndel, G.M., and van Lier, R.A. (1996). The seven-span transmembrane receptor CD97 has a cellular ligand (CD55, DAF). J. Exp. Med. *184*, 1185–1189.

Hoffman, B.D., Grashoff, C., and Schwartz, M.A. (2011). Dynamic molecular processes mediate cellular mechanotransduction. Nature *475*, 316–323.

Kirfel, G., Rigort, A., Borm, B., and Herzog, V. (2004). Cell migration: mechanisms of rear detachment and the formation of migration tracks. Eur. J. Cell Biol. *83*, 717–724.

Kishore, A., Purcell, R.H., Nassiri-Toosi, Z., and Hall, R.A. (2016). Stalk-dependent and stalk-independent signaling by the adhesion G protein-coupled receptors GPR56 (ADGRG1) and BAI1 (ADGRB1). J. Biol. Chem. *291*, 3385–3394.

Kubitschke, H., Schmauss, J., Nnetu, K.D., Warmt, E., Stange, R., and Kaes, J. (2017). Actin and microtubule networks contribute differently to cell response for small and large strains. New J. Phys. *19*, 093003.

Langenhan, T., Aust, G., and Hamann, J. (2013). Sticky signaling—adhesion class G protein-coupled receptors take the stage. Sci. Signal. *6*, re3.

Lee, H.J., and Zheng, J.J. (2010). PDZ domains and their binding partners: structure, specificity, and modification. Cell Commun. Signal. *8*, 8.

Li, Z., Zhang, C., Chen, L., Li, G., Qu, L., Balaji, K.C., and Du, C. (2016). E-cadherin facilitates protein kinase D1 activation and subcellular localization. J. Cell. Physiol. *231*, 2741–2748.

Liebscher, I., Schön, J., Petersen, S.C., Fischer, L., Auerbach, N., Demberg, L.M., Mogha, A., Cöster, M., Simon, K.U., Rothemund, S., et al. (2014). A tethered agonist within the ectodomain activates the adhesion G protein-coupled receptors GPR126 and GPR133. Cell Rep. *9*, 2018–2026.

Lin, H.H., Chang, G.W., Davies, J.Q., Stacey, M., Harris, J., and Gordon, S. (2004). Autocatalytic cleavage of the EMR2 receptor occurs at a conserved G protein-coupled receptor proteolytic site motif. J. Biol. Chem. *279*, 31823–31832.

Mattila, P.K., Batista, F.D., and Treanor, B. (2016). Dynamics of the actin cytoskeleton mediates receptor cross talk: An emerging concept in tuning receptor signaling. J. Cell Biol. *212*, 267–280.

Möller, B., Piltz, E., and Bley, N. (2014). Quantification of actin structures using unsupervised pattern analysis techniques. Proceedings of the International Conference on Pattern Recognition *1*, 3251–3256.

O'Neill, A.K., Gallegos, L.L., Justilien, V., Garcia, E.L., Leitges, M., Fields, A.P., Hall, R.A., and Newton, A.C. (2011). Protein kinase Cα promotes cell migration through a PDZ-dependent interaction with its novel substrate discs large homolog 1 (DLG1). J. Biol. Chem. *286*, 43559–43568.

Okajima, D., Kudo, G., and Yokota, H. (2010). Brain-specific angiogenesis inhibitor 2 (BAI2) may be activated by proteolytic processing. J. Recept. Signal Transduct. Res. *30*, 143–153.

Paavola, K.J., Stephenson, J.R., Ritter, S.L., Alter, S.P., and Hall, R.A. (2011). The N terminus of the adhesion G protein-coupled receptor GPR56 controls receptor signaling activity. J. Biol. Chem. *286*, 28914–28921.

Petersen, S.C., Luo, R., Liebscher, I., Giera, S., Jeong, S.J., Mogha, A., Ghidinelli, M., Feltri, M.L., Schöneberg, T., Piao, X., and Monk, K.R. (2015). The adhesion GPCR GPR126 has distinct, domain-dependent functions in Schwann cell development mediated by interaction with laminin-211. Neuron *85*, 755–769.

Römpler, H., Yu, H.T., Arnold, A., Orth, A., and Schöneberg, T. (2006). Functional consequences of naturally occurring DRY motif variants in the mammalian chemoattractant receptor GPR33. Genomics *87*, 724–732.

Salzman, G.S., Ackerman, S.D., Ding, C., Koide, A., Leon, K., Luo, R., Stoveken, H.M., Fernandez, C.G., Tall, G.G., Piao, X., et al. (2016). Structural basis for regulation of GPR56/ADGRG1 by its alternatively spliced extracellular domains. Neuron *91*, 1292–1304.

Salzman, G.S., Zhang, S., Gupta, A., Koide, A., Koide, S., and Araç, D. (2017). *Stachel*-independent modulation of GPR56/ADGRG1 signaling by synthetic ligands directed to its extracellular region. Proc. Natl. Acad. Sci. USA *114*, 10095–10100.

Scholz, N., Gehring, J., Guan, C., Ljaschenko, D., Fischer, R., Lakshmanan, V., Kittel, R.J., and Langenhan, T. (2015). The adhesion GPCR latrophilin/CIRL shapes mechanosensation. Cell Rep. *11*, 866–874.

Scholz, N., Guan, C., Nieberler, M., Grotemeyer, A., Maiellaro, I., Gao, S., Beck, S., Pawlak, M., Sauer, M., Asan, E., et al. (2017). Mechano-dependent signaling by latrophilin/CIRL quenches cAMP in proprioceptive neurons. eLife *6*, e28360.

Sivaramakrishnan, S., Schneider, J.L., Sitikov, A., Goldman, R.D., and Ridge, K.M. (2009). Shear stress induced reorganization of the keratin intermediate filament network requires phosphorylation by protein kinase C zeta. Mol. Biol. Cell *20*, 2755–2765.

Stacey, M., Chang, G.W., Davies, J.Q., Kwakkenbos, M.J., Sanderson, R.D., Hamann, J., Gordon, S., and Lin, H.H. (2003). The epidermal growth factor-like domains of the human EMR2 receptor mediate cell attachment through chondroitin sulfate glycosaminoglycans. Blood *102*, 2916–2924.

Stoveken, H.M., Hajduczok, A.G., Xu, L., and Tall, G.G. (2015). Adhesion G protein-coupled receptors are activated by exposure of a cryptic tethered agonist. Proc. Natl. Acad. Sci. USA *112*, 6194–6199.

Sun, Z., Guo, S.S., and Fässler, R. (2016). Integrin-mediated mechanotransduction. J. Cell Biol. *215*, 445–456.

Takeichi, M. (2014). Dynamic contacts: rearranging adherens junctions to drive epithelial remodelling. Nat. Rev. Mol. Cell Biol. *15*, 397–410.

Wang, T., Ward, Y., Tian, L., Lake, R., Guedez, L., Stetler-Stevenson, W.G., and Kelly, K. (2005). CD97, an adhesion receptor on inflammatory cells, stimulates angiogenesis through binding integrin counterreceptors on endothelial cells. Blood *105*, 2836–2844.

Ward, Y., Lake, R., Yin, J.J., Heger, C.D., Raffeld, M., Goldsmith, P.K., Merino, M., and Kelly, K. (2011). LPA receptor heterodimerizes with CD97 to amplify LPA-initiated RHO-dependent signaling and invasion in prostate cancer cells. Cancer Res. *71*, 7301–7311.

Wilde, C., Fischer, L., Lede, V., Kirchberger, J., Rothemund, S., Schöneberg, T., and Liebscher, I. (2016). The constitutive activity of the adhesion GPCR GPR114/ADGRG5 is mediated by its tethered agonist. FASEB J. *30*, 666–673.

Wobus, M., Vogel, B., Schmücking, E., Hamann, J., and Aust, G. (2004). N-glycosylation of CD97 within the EGF domains is crucial for epitope accessibility in normal and malignant cells as well as CD55 ligand binding. Int. J. Cancer *112*, 815–822.

Yang, Q., Zhang, X.F., Van Goor, D., Dunn, A.P., Hyland, C., Medeiros, N., and Forscher, P. (2013). Protein kinase C activation decreases peripheral actin network density and increases central nonmuscle myosin II contractility in neuronal growth cones. Mol. Biol. Cell *24*, 3097–3114.

Yonemura, S., Wada, Y., Watanabe, T., Nagafuchi, A., and Shibata, M. (2010). Alpha-catenin as a tension transducer that induces adherens junction development. Nat. Cell Biol. *12*, 533–542.